Influence of 2-D/3-D Urban Morphology on Diurnal Land Surface Temperature From the Perspective of Functional Zones

Qianmin Zhang, Jun Yang, Xinyue Ma, Jiaxing Xin, Jiayi Ren, Wenbo Yu, Xiangming Xiao, and Jianhong Xia

***Abstract*—Optimizing the spatial distribution of urban functional zones (UFZs) effectively improves the thermal environment. This study utilized an enhanced regression tree model and relied on Ecosystem Spaceborne Thermal Radiometer Experiment data to analyze the relative contributions and marginal effects of 2-D/3-D urban morphological factors on the diurnal land surface temperature (LST) in Shenyang, China. The results showed that public and residential areas dominated Shenyang's UFZs. The temperature in industrial areas was the highest during the day, and residential and commercial functional areas are high-temperature concentration areas. Furthermore, the effects of the urban spatial morphology on the LST differed between diverse time points and UFZs. The digital elevation model and the normalized difference vegetation index contributed significantly to daytime and nighttime LSTs. Construction indicators, such as the normalized difference built-up index and the proportion of construction land, significantly impacted commercial services. Residential daytime LST had a large contribution value, and the sum of its contribution rates reached approximately 30%. Population greatly contributed to the nighttime LST of the industrial and residential zones, accounting for 16.77% and 22.06%, respectively. Vegetation contributed to the cooling effect on daytime LST in summer, especially in industrial areas, contributing 29.79%. In addition, 3-D indicators, such as building height and building density, contributed to diurnal LST. Finally, when the proportion of construction land reached approximately 45%, it negatively affected LST. In this study, the main factors affecting day and night LSTs were identified, and this work acts as a relevant strategic reference for alleviating the urban heat island effect.**

***Index Terms*—Boosted regression tree, diurnal surface temperature, urban functional zones (UFZs), urban morphology.**

I. Introduction

In THE process of urban expansion and development, human activities have changed the natural surface of land, and the impervious areas and the number of building have increased sharply, exacerbating the heat island effect [1]. The urban heat island (UHI) results from urban areas experiencing elevated temperatures compared to surrounding rural areas, and this is influenced by alterations in urban surface features and human activities [2], which contributes to significant issues, including a deterioration in worsened air quality, heightened energy usage, and alterations in vegetation phenology [3]. Residents in urban areas experiencing persistent high temperatures are at an increased risk of developing cardiovascular and respiratory diseases [4]. Therefore, studying the driving mechanisms of the UHI effect is crucial for responding to climate change and achieving resilient urban development.

Many studies have analyzed the driving mechanisms of the UHI effect. Liu et al. [5] found that with the acceleration of urban construction and urbanization, the intensity of UHIs had also increased, and Beijing had experienced a temperature increase at a rate of 0.31 °C per decade over the previous 40 years. In addition, Oke [6] categorized the concept of the UHI into three components: canopy, boundary layer, and land surface layer. With the rapid development of remote sensing, land surface temperature (LST) has been widely studied, and it is known to be intrinsically related to human lives [7], [8], [9]. This is associated with seasons, time, vegetation fraction, water area, the proportion of impervious areas, and population (POP) density [10], [11], [12], [13], [14].

Satellite remote sensing observations have the advantages of wide coverage and regular return visits and have been widely used to produce different surface temperature products at multiple scales with different spatial resolutions [15]. The Ecosystem Spaceborne Thermal Radiometer Experiment (ECOSTRESS), launched on 29 June 2018, provides regular monitoring of LST data for various times throughout the day and night with a

Received 30 June 2024; revised 14 August 2024; accepted 3 September 2024. Date of publication 6 September 2024; date of current version 30 September 2024. This work was supported in part by the Liaoning Revitalization Talents Program under Grant XLYC2202024, in part by the Fundamental Research Funds for the Central Universities under Grant N2111003, in part by the Basic Scientific Research Project (Key Project) of the Education Department of Liaoning Province under Grant LJKZ0964, and in part by the Fundamental Research Funds for the Central Universities under Grant N2411001. *(Corresponding author: Jun Yang.)*

Qianmin Zhang and Xinyue Ma are with the Urban Climate and Human Settlements Research Lab, Jangho Architecture College, Northeastern University, Shenyang 110169, China (e-mail: 2301575@stu.neu.edu.cn; womaxinyue@163.com).

Jun Yang is with the Urban Climate and Human Settlements Research Lab, Jangho Architecture College, Northeastern University, Shenyang 110169, China, and also with the Human Settlements Research Center, Liaoning Normal University, Dalian 116029, China (e-mail: yangjun8@mail.neu.edu.cn).

Jiaxing Xin, Jiayi Ren, and Wenbo Yu are with the School of Humanities and Law, Northeastern University, Shenyang 110169, China (e-mail: 2310012@stu.neu.edu.cn; 2210011@stu.neu.edu.cn; 2110013@stu.neu.edu.cn).

Xiangming Xiao is with the School of Biological Sciences, University of Oklahoma, Norman, OK 73019 USA (e-mail: xiangming.xiao@ou.edu).

Jianhong Xia is with the School of Earth and Planetary Sciences, Curtin University, Perth, WA 6845, Australia (e-mail: c.xia@curtin.edu.au).

Digital Object Identifier 10.1109/JSTARS.2024.3455791

temporal and spatial resolution of 3–5 days and 70 m, respectively [16], [17]. These data derive LST and emissivity from five thermal infrared bands, which can be used to identify the factors influencing diurnal LST changes and provide time-series data support for UHI mitigation strategies [18]. Although the use of ECOSTRESS in thermal environment studies is currently relatively limited, it has shown great potential in providing high-resolution thermal data for urban heat environment analysis [19]. For instance, Lin et al. [20] used ECOSTRESS data to study the spatiotemporal connection between urban morphology and day and night surface temperature under different local climate zone classification frameworks in Fuzhou City based on ECOSTRESS data. In addition, some studies have explored the differences between diurnal and seasonal LSTs in Beijing [21].

LST is intricately linked with urban spatial form (USF) indicators from both 2-D and 3-D viewpoints, and some studies have started to focus on the impact of 3-D morphology on LST [22]. Three-dimensional buildings enhance the absorption of solar radiation absorption and diminish natural ventilation within cities, leading to intensified urban heat accumulation [23], [24], [25]. Han et al. [26] found that 3-D indicators significantly influenced surface temperature during the cold seasons, and that building coverage, the ratio of tall buildings, and the standard deviation of building heights consistently had the greatest impact. However, related research needs to focus on how 2-D and 3-D morphological indicators affect the diurnal and noctule surface temperature.

Urban functional zones (UFZs) are the basic units associated with social and economic activities and resource allocation, and they are intrinsically related to people's living needs. They are affected by natural conditions, social and economic development levels, policy planning, and other factors, which in turn affect the urban layout [27], [28]. The interaction between the USF and the thermal environments in different functional areas can result in ecological problems and affect human health [29]. Prior studies have primarily investigated the correlation between the USF and LST across various scales: regional, urban, block, and grid [30], [31], [32], [33]. For instance, An et al. [34] examined how urban green space characteristics affect LST at the block scale. Nevertheless, studies have shown that the contributions of UFZs to LST differ. Several studies have explored the link between USFs and LST through the lens of UFZs, revealing variations in the significance of USF on LST [35], [36]. For instance, Chen et al. [37] found that the LST within man-made functional areas is higher than that of the natural area. However, studies have also shown that the contributions of UFZs to LST differ.

In addition, most studies have focused on the correlation between single variables and have ignored the marginal effects of various parameters on LST. The marginal effect of a variable refers to the dynamic relationship between the independent variable and the dependent variable when other variables remain unchanged when the independent variable increases. In this respect, uncovering the marginal effect makes it possible to elucidate the nonlinear relationship between USF and LST and ultimately to optimize their configuration to effectively relieve the urban thermal environment [38]. To achieve this, boosting regression trees (BRTs) have been employed to effectively and scientifically derive the marginal effects of each driver and capture the significance of predictors [39], and they have been generally applied in urban outward expansion and thermal environment research. BRTs have been extensively applied in fields such as urban expansion and the thermal environment yield due to their ability to effectively extract marginal effects for each factor and their ability to highlight the significance of predictors.

To compensate for the limitations of the existing research, we chose the main urban area of Shenyang to examine factors affecting LST in various UFZs. Our specific study aims were as follows:

1) exploring the spatial differentiation between daytime and nighttime LST from the perspective of urban functional blocks;
2) employing the BRT model to discover the correlation of drivers and LST during daytime and nighttime;
3) analyzing the marginal effects of urban morphological variables and the contribution of USF on diurnal LST.

II. Materials

A. Study Area

Shenyang, the capital of Liaoning Province, serves as the central hub of the Shenyang Metropolitan Area (see Fig. 1). This area connects the Bohai Rim with northeast regions. Positioned between 122°25'9" E, 41°11'51" N and 123°48'24" E, 43°02'13" N, Shenyang has a temperate continental monsoon climate with distinct seasons. The climate features mild and windy springs and autumns, hot and rainy summers, and long cold winters. The average annual temperature is 8.4 °C, with temperatures ranging from –35 to 36 °C throughout the year. The average annual precipitation is 672 mm, with the majority of rainfall occurring between June and September. Prevailing winds are generally from the west throughout the year, with southwestern winds dominant in spring and summer. The total annual sunshine hours and accumulated temperature above 10 °C are 2550.7 h and 3488 °C, respectively. As an important industrial base in China, Shenyang has experienced a period of rapid urbanization and has faced the threat of extreme weather in recent years. As such, it can be used as a reference for the development of cities with similar development backgrounds. The study area is the urban center of Shenyang, including the Dadong, Heping, Huanggu, Hunnan, Shenbei, Shenhe, Sujiatun, Tiexi, and Yuhong districts.

B. Data Sources

This study made use of spatial data from multisources (see Table I). Specifically, to obtain and analyze analysis-ready data cases, we utilized ECOSTRESS level 2 products acquired through NASA's tool [40]. We chose the LST of the four hottest months (June–September) in Shenyang as the research object. We utilized four high-quality images without cloud cover from 30 August 2023, 1 September 2019, 6 August 2022, and 14 September 2023. Point-of-interest (POI) data were derived from the Amap Open Platform [41], [42]. Each POI dataset provided detailed attribute information (such as longitude and latitude,

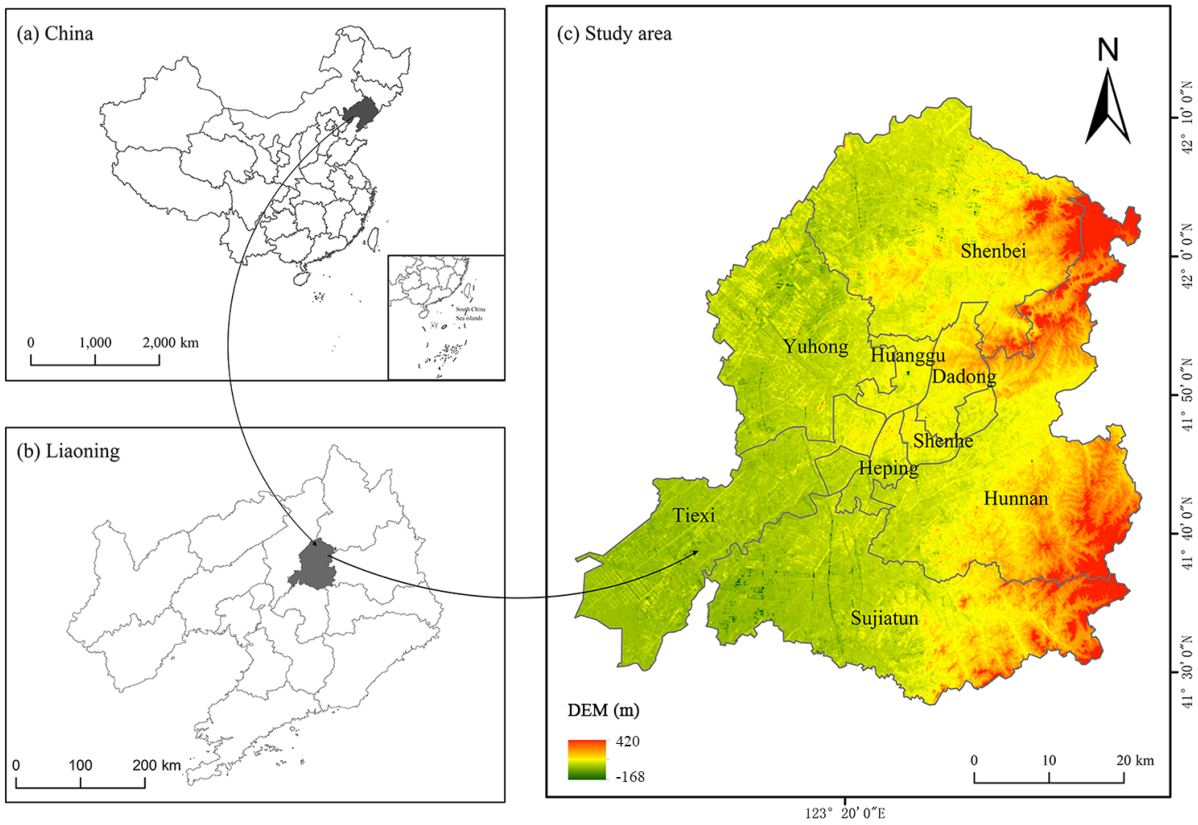

Fig. 1. Location of the study area. (a) Location of the Liaoning Province in China. (b) Location of the study area in the Liaoning Province. (c) The digital elevation model (DEM) of the study area.

TABLE I
DATA DESCRIPTION

Type of data	Time	Resolution	Data source
ECOSTRESS data	2019–2023	70 m	https://appeears.earthdatacloud.nasa.gov/ [40]
Point-of-interest data	2022		Amap Open Platform API Port [41], [42]
Digital elevation model	2020	30 m	Geospatial Data Cloud (http://www.gscloud.cn/search)
Land use	2020	30 m	CLCD (http://doi.org/10.5281/zenodo.4417809) [44]
Building	2018	-	Baidu API (https://lbs.amap.com/) [43]
Population	2020	100 m	Data from the seventh national census (https://figshare.com/s/d9dd5f9bb1a7f4fd3734) [45]
Tree height	2019	-	ftp://share.3decology.org

name, address, and type, combined with 200-m grid data), which was used to identify UFZs in the city. Data on buildings, including building area and number of floors, were acquired from the Baidu map service platform and used for building index calculations [43]. Land-use data from the China Land Cover Dataset (CLCD) were used to calculate landscape indicators [44], and POP data were obtained from the seventh national census of 2020 [45].

III. METHODS

A. Identification of UFZs

Fig. 2 is a technical roadmap, which includes the acquisition of daytime and nighttime surface temperature, identification of urban functional areas, identification of two-dimensional/three-dimensional factors, and related statistical analysis. Urban function is determined by external influences and a city's internal organizational structure, and identifying the distribution characteristics of UFZs is important for urban development and spatial resource allocation [46]. Some studies have used remote sensing images and nighttime light data to classify urban land use; however, they have not considered the socioeconomic attributes of surface objects or the type and intensity of human activities [47], [48], [49], [50]. With the widespread application of big data in the socioeconomic and urban planning fields in recent years, many scholars have implemented UFZ divisions based on POI, social media, mobile phone positioning, and public transportation data. Among them, POI data have a large sample size and rich information, representing the distribution of functional nodes on the urban microscale. They can indicate the intensity of human activity heat sources to realize the division of UFZs [51], [52], [53]. In this study, we selected a 200×200 m grid to identify UFZs conducive to the expression of similarity. In accordance with the standards for urban land classification and planning construction (GB 50137-2011), the POI data were categorized into six categories: residential, road traffic, commercial service, public service, industry, and green space.

In identifying UFZs, the frequency density and type ratio of POIs within a research unit (POI feature vector) are often used to identify the urban functional arrangement and directly reflect

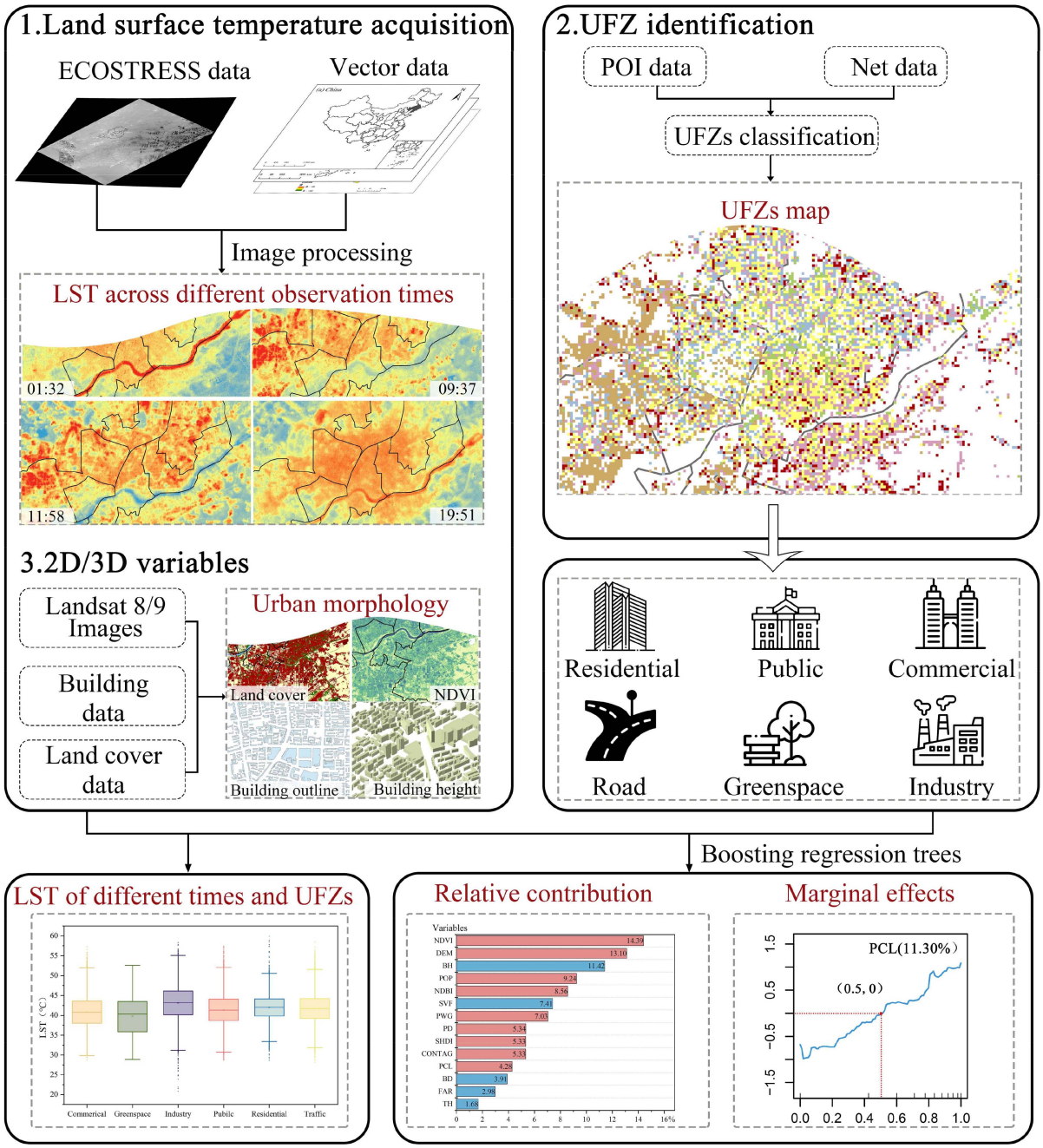

Fig. 2. Technical route.

the urban functional type

$$F_i = \frac{n_i}{S_I}, \quad i = 1, 2 \ldots, 6. \tag{1}$$

To facilitate comparison between different POI types, the CR vector was employed to indicate the percentage of each POI type within a unit based on its density

$$C_i = \frac{F_i}{\sum_{i=1}^{6} F_i} \times 100\%, \quad i = 1, 2, \ldots, 6. \tag{2}$$

In (1) and (2), i represents the POI type, n_i and S_i denote the count and the aggregate count of the ith type of POI in the research unit, F_i is described as the ith type of POI frequency density in the overall count of POIs of this type, and C_i indicates the frequency density of the ith type of POI accounting for the frequency density of all types of POI in the research unit.

When classifying the type, researchers generally select 50% as the basis for classification. If the CR vector value is greater than or equal to 50%, the unit is defined as a single UFZ [54]. Table II lists the classification of POI data.

B. ECOSTRESS Data

The ECOSTRESS project measures the LST of vegetation to understand water demand. Its application areas have expanded

TABLE II
POI DATA CLASSIFICATION

Primary classification	Secondary classification	Quantity	Proportion
Residential	Business Residence, Accommodation Services	2984	18.50%
Public Service Facility	Science and education culture，Exercise and fitness，Healthcare services，Government agencies and social groups，Life Services	3566	22.11%
Commercial Service Facility	Catering services, Shopping services, Hotel accommodation, financing institution, Leisure and entertainment, Domestic Services	2401	14.89%
Industry	Corporations	3401	21.09%
Road Traffic	Transportation services, Access facilities, Road supporting amenities	2752	17.06%
Green space	Famous Tourist Sites	1024	6.35%

since its launch, and it plays important roles in the UHI effects, abnormal weather monitoring, and mineral geological exploration. Previous studies have indicated strong agreement between the ECOSTRESS LST product and LST data obtained from established thermal infrared instruments [55], [56], [57]. The root-mean-square error at 14 validation points around the world is 1.07 K, the mean absolute error is 0.40 K, and $R^2 >$ 0.988. This research utilized ECOSTRESS data to collect the LST for various dates and periods within the study region. The four study times were 01:32 on 30 August 2023, 09:37 on 1 September 2019, 11:58 on 6 August 2022, and 19:56 on 14 September 2023. The background temperature ranges of the four dates were 7–23, 13–45, 12–61, and 6–23 °C, respectively.

C. Urban Morphological Factors

Studying the effect of 2-D/3-D urban forms on LST is important to respond to climate change [58]. The 2-D/3-D parameters primarily included land cover, architectural form, landscape pattern, POP, and other related indicators [59]. To exclude the influence of factor collinearity, the variance inflation factor (VIF) was used for testing, and 14 factors with VIF < 10 were retained for subsequent analysis [60]. The distribution of urban form factors can be obtained by calculating the average value of the unit indicators in each functional area. The implications of each indicator are presented in Table III. Among them, the relevant indicators of landscape patterns include patch density, the Shannon diversity index, and the contagion index, which can fully describe structural characteristics and spatial configuration of landscape [61], [62]. In addition, the shape and structure of buildings significantly affect UHIs [63]. In this study, we selected relevant indicators, such as BH, BD, SVF, and floor area ratio (FAR) [64], [65]. POP density can also reflect the socioeconomic status of a region [66]. All the data were projected, clipped, and unified into 20 m $\times$ 20 m grid cells.

D. Statistical Analysis

To investigate the impact of various USF indicators on LST, we examined the correlation between these indicators and LST at four different time points. Unlike other analytical methods, the Spearman coefficient is more suitable for data with non-normal distributions. Moreover, the BRT is a statistical machine learning technique that advances a single model's predictive performance by integrating multiple models and combining their forecasted outcomes effectively [67]. The core of this method is its unique decision tree structure and boosting algorithm. Compared with other models, the BRT simplifies the consideration of complex interactions among independent variables by directly revealing influence of these variables and response patterns on the dependent variables [68]. Decision trees are widely favored due to their ability to present information in a clear and graphical format that is intuitive and easily understandable for users. In addition, BRT comprises flexible and diverse predictor variable types, including but not limited to numerical, binary, and categorical types, which greatly broadens the scope of its application. The BRT model is robust to monotonic transformations of predictors or measurement scales and can automatically screen out predictors with higher correlations, thus simplifying the screening process for candidate predictors. Boosting technology, integral to BRT, enhances prediction accuracy through iterative staged processes that progressively improve model performance [69], [70]. The BRT method generally excels in predicting and identifying interactions among multiple variables, effectively assessing the relative contribution and marginal effects of urban form on LST. It comprehensively evaluates variable influences [71].

IV. RESULTS

A. UFZ Identification Results

Fig. 3 illustrates an illustration depicting the segmentation of UFZs. The results of the confusion matrix show that the overall classification accuracy is 87.1%, and the Kappa coefficient is 0.843, reflecting strong consistency. The urban functional area recognition model thus has high accuracy and can be used as a reference for urban spatial structure characteristics. Commercial public service and residential POIs were mainly fixed on the central area; industrial POIs were fixed on the surrounding areas, mainly in the Tiexi District; transportation POIs were predominantly clustered along major roads, airports, and high-speed rail stations. Green space POIs were scattered. In total, 17 538 valid grids were obtained. Residential, public service, and industrial land proportions were relatively large, with public service land accounting for the largest proportion (22.11%) followed by industrial land (21.09%). Green space land accounted for 6.35%, and the overall green space configuration must be strengthened.

TABLE III
URBAN MORPHOLOGICAL FACTORS

Type	Indicator variables	Calculation formula	Implication
2D	Patch density (PD)	$PD = \frac{n_i}{S}$	Represents different landscape patch densities in a cell.
	Shannon diversity index (SHDI)	$SHDI = -\sum_{i=1}^{n} P_i \times \ln(P_i)$	Represents the ratio of each patch type across all patches, multiplied by the sum of these ratios.
	Contagion index (CONTAG)	$CONTAG = \left[1 + \frac{\sum_{i=1}^{m}\sum_{k=1}^{m}\left[(P_i)\left(\frac{g_{ik}}{\sum_{k=1}^{m} g_{ik}}\right)\right]\left[\ln(P_i)\left(\frac{g_{ik}}{\sum_{k=1}^{m} g_{ik}}\right)\right]}{2\ln(m)}\right](100)$	Represents the degree to which each patch type is clustered or spread across the landscape.
	Proportion of woodland and grass (PWG)	$PWG = \frac{\sum_{i=1}^{n} \frac{G_i}{S_i}}{n}$	Represents the proportion of forest and grassland areas in each cell.
	Proportion of construction land (PCL)	$PCL = \frac{\sum_{1}^{n} \frac{A_i}{S_i}}{n}$	Represents the percentage of land area designated for construction within each cell.
	Digital elevation model (DEM)	-	Represents the average elevation of the DEM within each grid cell.
	Normalized difference vegetation index (NDVI)	$NDVI = \frac{NIR - RED}{NIR + RED}$	Represents the mean NDVI value within each grid cell.
	Normalized difference built-up index (NDBI)	$NDBI = \frac{SWIR - NIR}{SWIR + NIR}$	Represents is the average NDBI value within each grid cell.
	Population (POP)	$POP = \sum_{i=1}^{n} \frac{P_n}{n}$	Represents the population in each cell.
3D	Building height (BH)	$BH = \frac{\sum_{i=1}^{n} H_i}{n}$	Represents the mean building height within each grid cell.
	Building density (BD)	$BD = \sum_{i=1}^{n} \frac{s_i / S}{n}$	Represents the density of buildings within each cell.
	Mean tree height (TH)	$TH = \sum_{i=1}^{n} \frac{H_i}{n}$	Represents the average height of trees in each cell.
	Floor area ratio (FAR)	$FAR = \sum_{i=1}^{n} \frac{F_i * H_i}{A}$	Represents the proportion of total building area to total land area.
	Sky view factor (SVF)	$SVF = \frac{\sum_{i=1}^{n} SVF_i}{n}$	Represents the sky view factor in each cell.

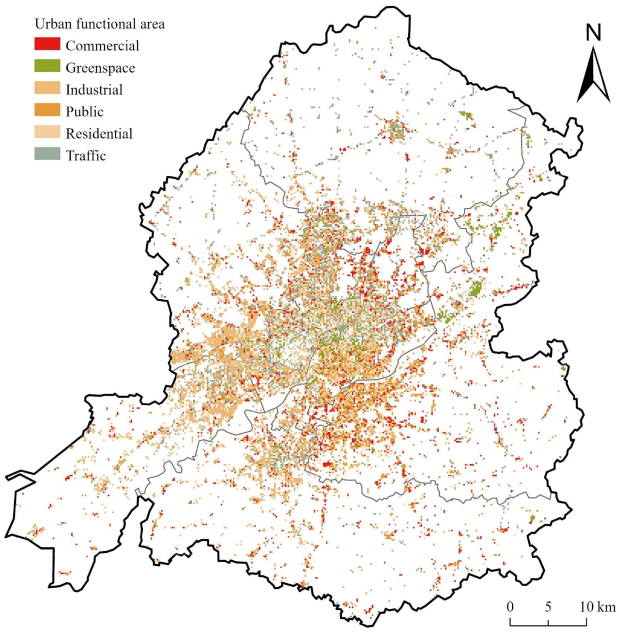

Fig. 3. UFZ identification results.

B. Spatial Distribution of Diurnal Surface Temperature

Table IV displays statistical data of LSTs at various observation times. Among the four study times, the lowest LST value appeared at 01:32, with an average LST of 14.5 °C. As the day progressed, the LST value increased, reaching 26.0 °C at 09:32, peaking at 36.1 °C at 11:58, and declining at 19:51 after sunset. The average LST was 16.2 °C.

The spatial variation in the daily average LST is shown in Fig. 4, where Fig. 4(a) and (d) shows the LST data obtained at night. Bodies of water exhibit the highest values. The LST in built-up areas was relatively high and tended to spread outward. As shown in Fig. 4(b), the average LST increased by 8 °C at 09:37. LSTs were significantly different at night, and the water body temperature was relatively low. With a rise in the impermeable surface temperature, LSTs in the western and southern regions of the study area increased rapidly, whereas they remained relatively high in the central region. At 11:58, this trend was further strengthened, and the LST was 10 °C higher than the average temperature in the morning, as shown in Fig. 4(c). The LST at 19:51 is shown in Fig. 4(d), where the high-temperature aggregation phenomenon is evidently alleviated to a certain extent.

TABLE IV
STATISTICS OF LST ACROSS FOUR OBSERVATION TIMES

Local time	Land surface temperature（℃）			
	Mean	Minimum	Maximum	Standard deviations
01:32	14.5	7.8	23.7	1.5
09:37	26.0	13.6	45.3	2.8
11:58	36.1	13.0	61.5	4.8
19:51	16.2	6.7	23.5	2.0

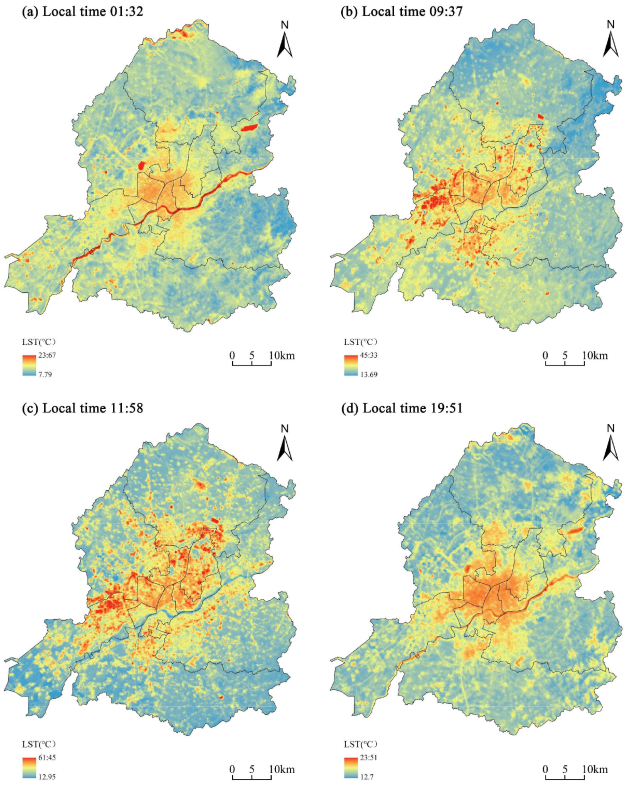

Fig. 4. Spatial distribution of diurnal and noctule LST in the study area. (a)–(d) Surface temperature information at 01:32, 09:37, 11:58, and 19:51, respectively.

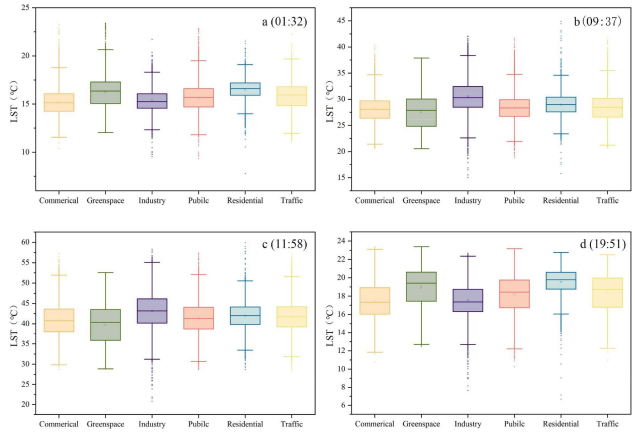

Fig. 5. Box plots of LST in different UFZs at four time points. (a)–(d) Maximum, minimum, median, and other related values of the surface temperature value in different functional areas at four times: 01:32, 09:37, 11:58, 19:51.

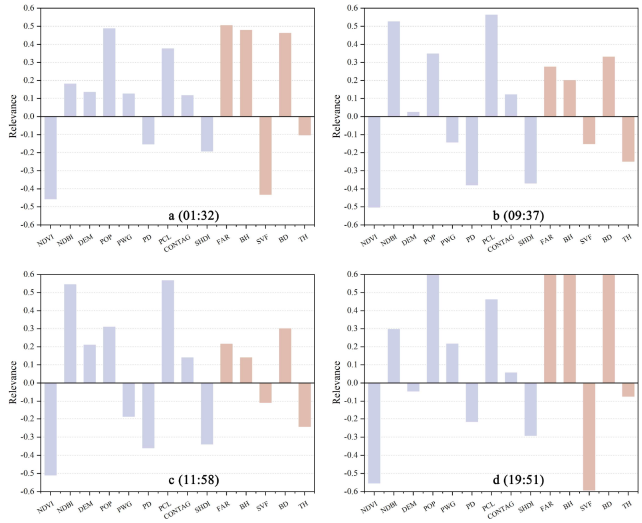

Fig. 6. Relevance between surface temperature and morphological factors at different time points. (a)–(d) Correlation index between USF factors and LST at 01:32, 09:37, 11:58, and 19:51, $p < 0.05$.

The differential changes in the LST among various UFZ types are shown in Fig. 5. At night, the temperature values of the commercial and industrial zones were lower, and higher temperature values were recorded in the green areas. During the day, the industrial zones quickly heated, reaching 43.1 °C at 11:58. The LST of zones with human activities, such as residential, commercial, and public services, were also relatively high. Green areas became cold island areas during the day, with mean LSTs of 27.5 °C and 39.8 °C at 09:37 and 11:58, respectively.

C. Relative Contribution of Urban 2-D/3-D Morphological Drivers to Diurnal LSTs

The effects of different urban morphology elements on LST during both day and night are exhibited in Figs. 6 and 7. BRT regression and Spearman correlation coefficients identified the direction of effects. If the Spearman correlation indicates a positive relationship, the overall contribution is positive, and vice versa. During the daytime, normalized difference built-up index (NDBI) and the proportion of construction land (PCL) were positively correlated with the daytime surface temperature. Two-dimensional morphological factors, such as digital elevation model (DEM) and the NDBI, impacted commercial and industrial zones more. In contrast, residential zones were affected by 3-D building forms such as BD. PCL was more important

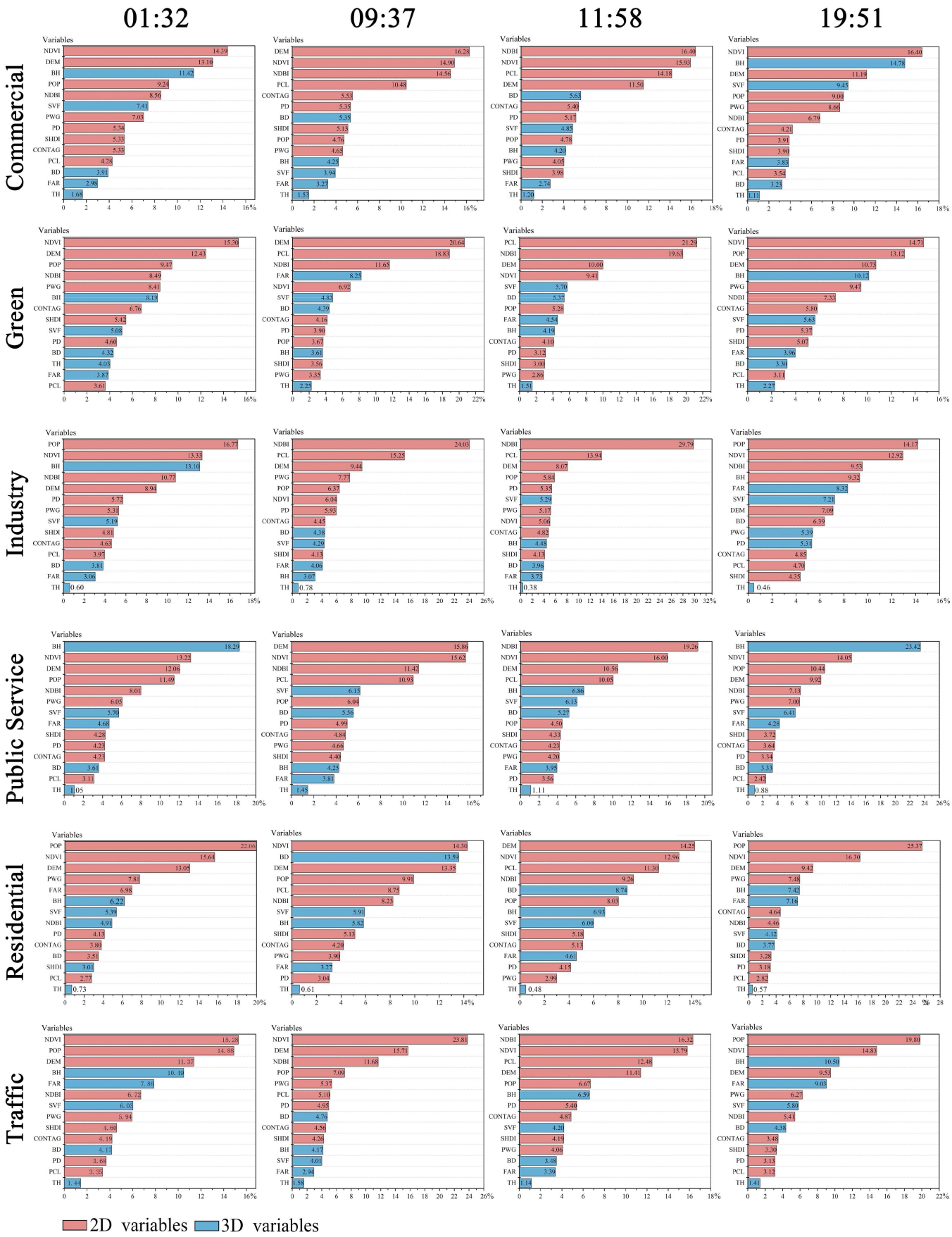

Fig. 7. Relative contribution of urban morphology factors to daytime and nighttime LSTs.

for green zones. At night, the normalized difference vegetation index (NDVI), POP, and other drivers predominantly influenced the LST across different UFZs within the city, and there was a significant negative correlation between SVF and night surface temperature. Furthermore, 3-D building indicators such as BH contributed significantly to residential zones. Building height and BD were important 3-D factors influencing the diurnal and noctule LST.

At 01:32, the NDVI contributed the most to the commercial, green, and transportation zones at 14.39%, 15.30%, and 15.28%, respectively. POP had a greater impact in the industrial and residential zones (16.77% and 22.06%, respectively). Building height was an important 3-D factor affecting the public service zones, reaching 18.29%.

At 09:37, the DEM had the highest impact on UFZs, such as commerce, green space, and public services, at 16.28%, 20.64%, and 15.86%, respectively. Compared to 01:32, the importance of the PCL in the LST increased. Considering the green space UFZ as an example, the contribution increased from 3.61% to 18.83%. The impact of BD on residential areas increased significantly, from 3.51 to 13.59%. The NDBI has become an important 2-D-factor affecting industrial zones, with a contribution value of 24.03%, and its impact on other UFZs increased.

At 11:58, NDBI became the dominant factor affecting various UFZs, and its importance in commerce, industry, public services, and transportation zones was 16.40%, 29.79%, 19.26%, and 16.32%, respectively. The impact of PCL on various UFZs increased, and its contribution value to the green space UFZ reached 21.29%.

At 19:51, the impacts of the NDVI and POP recovered. Among them, NDVI was the largest 2-D morphological factor affecting commercial and green space zones, at 16.40% and 14.71%, respectively. POP was the most important factor for industrial, residential, and transportation zones, reaching 14.17%, 25.37%, and 19.80%, respectively. At night, the contribution of the BH increased. Compared with at 11:58, the contribution value to the public service UFZ increased from 6.86% to 23.42%, becoming the most important 3-D morphological factor affecting the UFZ. In addition, SVF was an important factor affecting commercial UFZ, contributing 9.45%. The impact value of the FAR on the industrial UFZ increased by 4.59% compared to 11:58.

D. Marginal Effects of 2-D/3-D Urban Morphological Drivers on Diurnal LSTs

To compare the impact of the relevant parameters of different UFZs on LST, two extreme values were selected at 01:32 and 11:58. Considering that the other two time points, 09:37 and 19:51, had certain similarities with these, four significant indicators were selected according to their contribution to LST, considering their marginal effects on LST. At 01:32, four indicators, NDVI, DEM, BH, and POP, were selected, with a total contribution rate of 45.69–56.97%. At 11:58, NDBI, NDVI, PCL, and DEM were selected, with a total contribution rate of 47.77–60.33%. The horizontal and vertical axes in Figs. 8 and 9 reflect the extent of variation of each driver and its effect on LST. The vertical coordinates >0, 0, and <0 indicate positive, no, and negative correlations with LST, separately. The larger the absolute value, the greater the impact value.

At 11:58, LST reached its peak value of the four research moments. The NDBI showed a crucial warming effect in various UFZs, and PCL also played a crucial role in affecting LST. The proportion of constructed land of 40–50% indicated the shift, beginning with a negative correlation and concluding with a positive correlation. A crucial warming effect was observed as the PCL values increased. In urban planning, it is advisable to avoid blind expansion to mitigate the heat island effect. The NDVI represents vegetation coverage; greater values signify abundant greenery and shaded regions. When the NDVI value was $>40\%$, it had a strong cooling effect, particularly in industrial areas where the threshold was as low as 10%.

At 01:32, when the NDVI was approximately 0.4, it exhibited a negative correlation with LST, significantly cooling public activity areas such as businesses, public services, and transportation. When the DEM was 60–90 m, a positive link with LST was seen due to the increased human activity in those areas. Beyond this boundary, the two values exhibited a negative correlation. Because of the need for terrain flatness in industrial areas, this value was advanced to 28 m. The BH critical point of UFZs with public activities, such as commerce, public services, residences, and green spaces, was 50–60 m, while that of industrial and transportation zones was 10–20 m. When this value was exceeded, a warming effect occurred. Therefore, in urban planning administration, reducing the construction of super high-rise buildings is crucial for enhancing perceived comfort.

V. Discussion

A. Spatiotemporal Heterogeneity of Diurnal LST Variations

Spatiotemporal variations in daytime and nighttime LSTs exhibited a distinct inverted U-shaped trend. At night, high-temperature zones were mainly located in water bodies, whereas low-temperature zones were primarily found in areas with dense vegetation, such as the eastern mountains and hills. During the daytime, areas of vegetation also showed lower temperatures. Ibsen et al. [72] explored that in semiarid areas, the increased areas of vegetation, especially tree canopy, play an important role in reducing solar radiation and lowering surface temperature. The absence of solar radiation at night also has the same effect, which is consistent with our results. Water bodies gradually transitioned from being cold sources to hot spots. At the same time, the LST of impermeable surfaces in built-up areas increased rapidly, with the LST values rising from low to high. The highest LST in the four time periods studied occurred at 11:58, further strengthening this trend. This phenomenon occurred because materials such as building metals, which have low specific heat capacities, heat up quickly in sunlight, and cool down rapidly after sunset, resulting in very high LSTs during the day, especially at noon, and lower LSTs at night [73], [74]. Water has a high specific heat capacity, so it warms much slower when absorbing equal amounts of heat energy; thus, it becomes a heat island area in the city during the day. The energy absorbed during

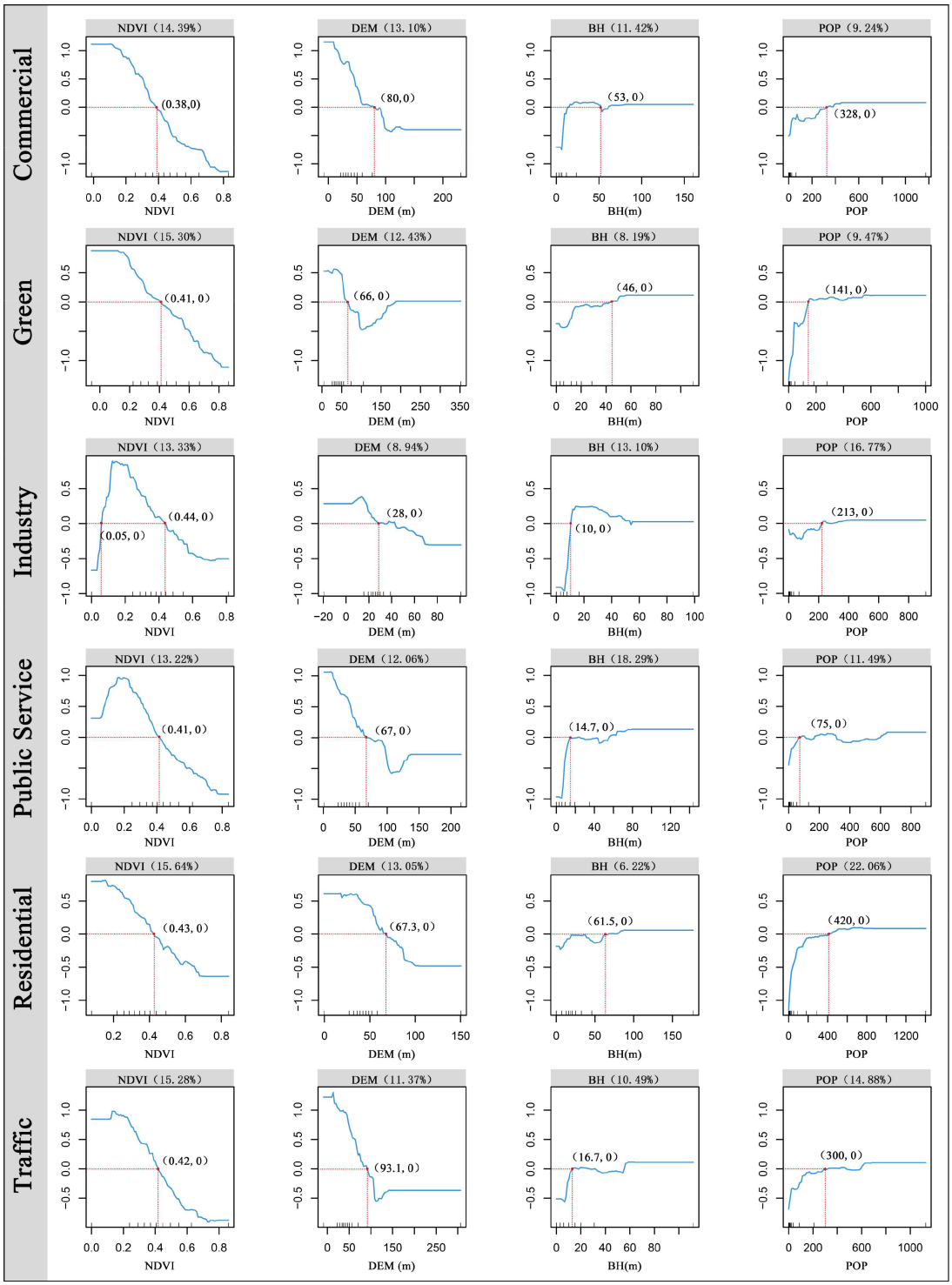

Fig. 8. Marginal effect of urban morphology drivers on LST at 01:32.

the day is gradually released at night, resulting in elevated LST values [75]. The cooling effect of water bodies has been further enhanced in riverside and coastal cities [76].

The LST variation between daytime and nighttime across various UFZs is shown in Fig. 4. During the day, the temperature in industrial areas was the highest. In this respect, the operation of industrial equipment generates a large amount of heat, causing the temperature to increase. Higher temperatures are typically found in residential, commercial, and public service areas [77], [78], [79], and this is primarily because UFZs consist of impermeable surfaces that heat up more quickly than natural surfaces, and they are also influenced by human activities. Chen et al. [80] found that public service facilities contribute the most to the thermal environment. Since the author used data from 2020,

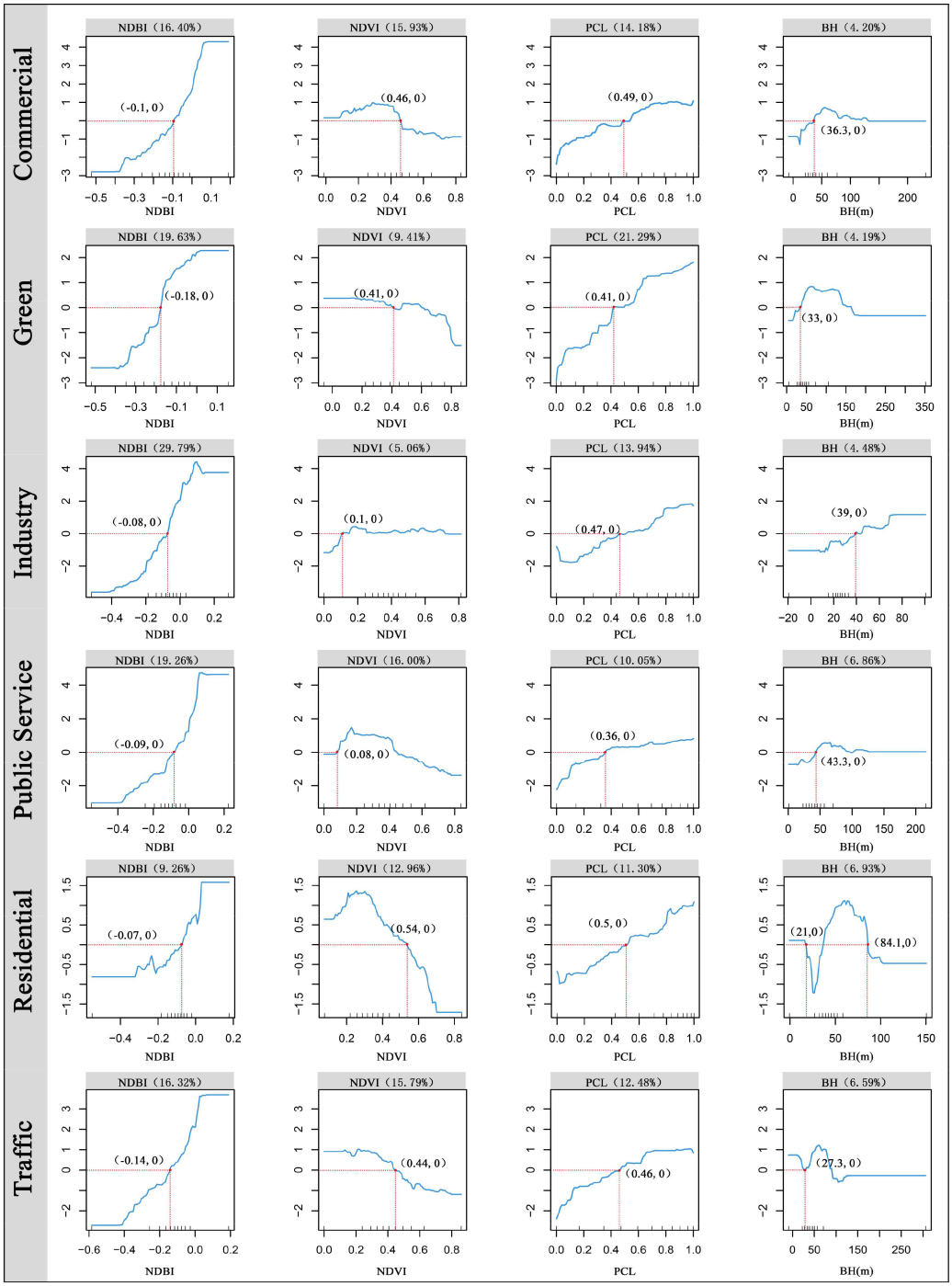

Fig. 9. Marginal effect of urban morphology drivers on LST at 11:58.

we speculate that due to factors such as the influence of health care, the artificial heat generated by public service facilities such as health care increased during this period. At present, the vitality of industrial and commercial facilities has recovered, so the impact of industrial facilities on the thermal environment has increased. We also found that the high-temperature phenomenon in the green spaces and squares was weak. This relates to the large-scale vegetation coverage enhancing the thermodynamic characteristics of the underlying surface, facilitating air cooling and circulation, and thereby exerting a substantial regulatory influence on LST, as determined in other studies.

B. Variations in the Impact of Urban Morphology on Diurnal LSTs Across Different UFZs

Some studies have drawn different conclusions when studying urban morphological factors using ECOSTRESS LST data. Lin et al. [81] believed that the anthropogenic heat in Fuzhou impacted LST at night. In contrast, in the present study, we found

that the relevant construction indicators had a greater impact during the daytime. Fuzhou is an inland city located near the eastern coast, whereas Shenyang is a city at a higher altitude located further inland. Therefore, the climate difference between the two locations is significant, especially when the humidity conditions differ. Shenyang is an industrial city with additional industrial heat production. Therefore, the daytime was affected more by anthropogenic heat.

Extensive studies have investigated how the USF influences the thermal environment, as well as the effects of 2-D/3-D morphology on LST [82]. Generally, 2-D drivers have a greater impact on daily LST variations than 3-D drivers. In this study, the impact of the 2-D drivers on daily LST variations tended to that of 3-D drivers. In comparison to previous studies, we determined that the DEM was the predominant factor affecting daytime LST; as altitude increases, variations in slope orientation and gradient impact how the surface absorbs solar heat energy, bringing about differences in LST, which consistent with previous reports [83]. In addition, the NDBI and PCL contributed significantly to the LST of the commercial, industrial, public service, and other zones. With the increase in human activities, the importance of indicators related to urban construction increased. Surface biophysical parameters, such as NDVI, contribute significantly to public service areas. Vegetation can evaporate water to keep the temperature low. These areas typically have extensive impermeable surfaces, which capture and retain solar radiation while limiting evapotranspiration, leading to higher LST levels. LST of public service facilities is more responsive to impermeable surfaces. Given the unique construction environment of commercial districts, numerous factors influence LST.

Chang et al. [84] discovered that POP was correlated more with nighttime surface temperature than daytime, and this is consistent with the results of our related study. In addition, POP was found to be an important factor affecting residential and industrial areas at night, which previous studies have not mentioned [85]. It is speculated that residents mostly rest at home at night, although people may work night shifts in factories. However, commercial, public service, and other areas are mostly closed at night; therefore, the impact is less. In addition, 3-D factors, such as BH and BD, are important influencers of daytime LST in functional areas such as residential and public services, because taller buildings can cast more shadows and affect LST simultaneously. However, Chen et al. [86] found that BH had a weakening effect on daytime LST in winter, which may have been due to a decrease in both the duration and intensity of sunlight, resulting in a significantly lower LST. Hence, the importance of 3-D morphological parameters is crucial when studying the thermal conditions of densely populated urban areas. Urban planning authorities need to strategically regulate building control indicators to mitigate heat absorption and alleviate UHIs.

C. Marginal Effects of Urban Morphology on Diurnal LSTs in Different UFZs

Although studies have analyzed the marginal effect of urban morphology and surface temperature, few have investigated the difference between day and night from the perspective of different functional areas. In this study, we made some new discoveries. Suthar et al. [87] found that the irregular increase in built-up areas was an important reason for the increase in surface temperature in summer. In this study, PCL and NDBI were two important warming factors during the day, and this is consistent with the results of previous studies. Significant positive correlations with LST reached 0.1 and 0.45, respectively. Therefore, the increase in construction on land should be strictly controlled in highly urbanized areas. Furthermore, the NDVI was an important cooling indicator affecting daytime and nighttime LST. Unlike observations in other studies, we found that the NDVI had a greater effect on industrial and public service areas, and the cooling effect was the most obvious when the NDVI was >0.1. Solar radiation can be blocked by expanding green areas and increasing vegetation coverage, leading to a better cooling effect. Chen et al. [88] found that the DEM was negatively correlated with LST. However, the present study found that the DEM had a complex effect on the daytime LST of zones such as residential and commercial services. When the DEM value was <20 m or >80 m, the transpiration between vegetation was strong, promoting air cooling. The LST in the middle area increased because of the concentration of human activities.

During daytime, when the BH increased, the heat exchange increased, and the LST was reduced to a certain extent; this aligns with the findings of other studies and is related to shaded areas reducing solar radiation [89]. However, unlike other studies, we found that the intensity of sunlight at night was more limited than during the day and solar radiation decreased accordingly; therefore, the opposite conclusion was drawn. When the BH was >40 m, it had a certain wind-shielding and heat-insulating effect and a positive correlation with the LST. However, the critical threshold differed [90], [91]. Mo et al. [92] found that when the building height was greater than 60 m, the cooling effect of residential areas was more significant. Some researchers believe that there may be a positive relationship between climate, horizontal distance, and the solar elevation angle between buildings [85], but relevant research is required.

D. Impact on Urban Planning and Management

The scientific planning of urban spatial layouts profoundly impacts the thermal environment. The gradient of urban expansion can be divided into the following three levels in this study: the first level is the urban center, including the southern part of Huanggu District, the eastern part of Yuhong District, the northern part of Heping District, the western part of Shenhe District, and the northern part of Hunnan District. These areas are mostly public activity areas, with more heat release and limited air circulation and heat mitigation capabilities. Considering the development density of the site and the land value, it is unlikely that major adjustments in the spatial structure will be made. However, a landscape regulation system for heat mitigation can be established by establishing a greening cooling system and increasing vegetation coverage. The second level is the northern

part of Huanggu District, the southwestern part of Yuhong District, the southwestern part of Dadong District, the eastern part of Shenhe District, the western part of Hunnan District, and the northeastern part of Tiexi District. These areas have a medium-level building density distribution and artificial heat release, with certain industrial activities and a relatively low greening rate. In these areas, the urban spatial structure can be appropriately adjusted and improved, a favorable air circulation environment can be created, and greening can be encouraged. In particular, the industrial area in Tiexi District can cool the environment by increasing the greening area and optimizing the industrial layout. The third level is the southern part of Shenbei New Area, the eastern part of Hunnan District, the northeastern part of Dadong District, the eastern part of Shenhe District, and the northwestern part of Sujiatun District. From the perspective of location, these areas are located at the edge of the built-up area where there is a low construction density. We found that NDBI and PCL were important influencing factors during the daytime. According to the relevant requirements of national land space planning, it is necessary to control the growth boundary of urban areas and improve resource utilization and structural adjustment through effective space. BH and BD were found to be the main 3-D factors affecting the daytime and nighttime surface temperature. Therefore, maintaining a reasonable building height difference and building density during the planning and construction of the new area can help to control the airflow between buildings, which would have a cooling effect on the area. It is important to consider spatial patterns to enable high-quality and sustainable advancements to be made.

E. Limitations

We explored how urban morphology affects diurnal LST. However, our work has certain limitations. Due to the particularity of the orbit of the International Space Station, the difficulty in obtaining nighttime LST data, and the influence of cloud cover, the number of available ECOSTRESS remote sensing images was highly limited. It was impossible to guarantee that the day and night surface temperatures belonged to the same day. Therefore, our data accuracy has produced certain errors. In future research, all-weather remote sensing data should be considered, or ground monitoring and numerical simulation technology should be combined to obtain surface temperature data with high temporal resolution. To enhance the comprehensiveness of this study, we could consider the heterogeneity of LST and urban morphology of different landforms and developmental backgrounds and extend this research to encompass other cities, thereby investigating both the general applicability and distinctive characteristics of the findings.

VI. Conclusion

In this article, we investigated the variability in LST across various UFZs. We used an enhanced regression tree model and ECOSTRESS summer daily variation data to examine how urban 2-D and 3-D morphology influences daily LST. The following are the principal conclusions that can be drawn from this study.

1) The UFZs of Shenyang are mainly residential and public service areas; among them, public service land accounts for the largest proportion, reaching 22.11%. And there was a clear spatial heterogeneity in the daytime and nighttime LST of the different UFZs in Shenyang's primary urban zones. At daytime, the temperature in the industrial area was the highest, reaching 43.1 °C at 11:58. The residential, commercial, and service areas were concentrated in high-temperature areas as well. Green squares indicate a significant cooling effect. At night, the water becomes a heat source in the city.
2) NDVI and DEM were important factors affecting various UFZs. Construction-related indicators, such as PCL and NDBI, significantly contributed to daytime LST, and their combined contribution to commercial and residential functional areas reaches about 30%. Nighttime POP is an important factor affecting LST in residential and industrial areas, with contribution rates of 22.06% and 16.77% at 01:32 respectively. In addition, 3-D factors, such as BH and BD, played a synergistic role with 2-D factors on LST.
3) With respect to the marginal effect, when PCL $>$ 45%, there was a substantial warming effect on the daytime and nighttime LST. Because of the appearance of building shadows, the effect of BH on LST showed variation during daytime and nighttime. There was noticeable cooling observed when the BH exceeded 40 m during the day. However, at night, as the BH increased, it had a warming impact on the LST after the critical point. NDVI has a significant cooling effect on each UFZs, especially the industrial functional area, where the threshold is 10%, and LST can be reduced by expanding green areas.

Urban planners can enhance the thermal environment through well-designed spatial layouts and strategic plans, fostering resilient urban growth. This study also provides valuable insights for guiding future decision making, planning, and strategies aimed at mitigating the UHI effect.

References

[1] S. Zhao, L. Da, Z. Tang, H. Fang, K. Song, and J. Fang, "Ecological consequences of rapid urban expansion: Shanghai, China," *Front. Ecol. Environ.*, vol. 4, no. 7, pp. 341–346, 2006, doi: 10.1890/1540-9295.
[2] T. R. Oke, "City size and the urban heat island," *Atmos. Environ.*, vol. 7, no. 8, pp. 769–779, Aug. 1973, doi: 10.1016/0004-6981(73)90140-6.
[3] J. Yang, Y. Zhan, X. Xiao, J. C. Xia, W. Sun, and X. Li, "Investigating the diversity of land surface temperature characteristics in different scale cities based on local climate zones," *Urban Climate*, vol. 34, Dec. 2020, Art. no. 100700, doi: 10.1016/j.uclim.2020.100700.
[4] P. Shahmohamadi, A. I. Che-Ani, I. Etessam, K. N. A. Maulud, and N. M. Tawil, "Healthy environment: The need to mitigate urban heat island effects on human health," *Procedia Eng.*, vol. 20, pp. 61–70, Jan. 2011, doi: 10.1016/j.proeng.2011.11.139.
[5] Y. Liu, Y. Xu, F. Weng, F. Zhang, and W. Shu, "Impacts of urban spatial layout and scale on local climate: A case study in Beijing," *Sustain. Cities Soc.*, vol. 68, May 2021, Art. no. 102767, doi: 10.1016/j.scs.2021.102767.
[6] T. R. Oke, "The heat island of the urban boundary layer: Characteristics, causes and effects," in *Wind Climate in Cities*, J. E. Cermak, A. G. Davenport, E. J. Plate, and D. X. Viegas, Eds., Dordrecht, The Netherlands: Springer, 1995, pp. 81–107.

[7] M. Aminipouri and A. Knudby, "Spatio-temporal analysis of surface urban heat island (SUHI) using MODIS land surface temperature (LST) for summer 2003–2012, A case study of The Netherlands," in *Proc. IEEE Geosci. Remote Sens. Symp.*, 2014, pp. 3192–3193, doi: 10.1109/IGARSS.2014.6947156.

[8] H. Li et al., "An operational split-window algorithm for generating long-term land surface temperature products from Chinese Fengyun-3 series satellite data," *IEEE Trans. Geosci. Remote Sens.*, vol. 61, 2023, Art. no. 5004514, doi: 10.1109/TGRS.2023.3315968.

[9] R. Li et al., "Land surface temperature retrieval from Sentinel-3A SLSTR data: Comparison among split-window, dual-window, three-channel, and dual-angle algorithms," *IEEE Trans. Geosci. Remote Sens.*, vol. 61, 2023, Art. no. 5003114, doi: 10.1109/TGRS.2023.3288584.

[10] A. Azhdari, A. Soltani, and M. Alidadi, "Urban morphology and landscape structure effect on land surface temperature: Evidence from Shiraz, a semi-arid city," *Sustain. Cities Soc.*, vol. 41, pp. 853–864, Aug. 2018, doi: 10.1016/j.scs.2018.06.034.

[11] I. M. Parvez, Y. A. Aina, and A.-L. Balogun, "The influence of urban form on the spatiotemporal variations in land surface temperature in an arid coastal city," *Geocarto Int.*, vol. 36, no. 6, pp. 640–659, Mar. 2021, doi: 10.1080/10106049.2019.1622598.

[12] J. Song, W. Chen, J. Zhang, K. Huang, B. Hou, and A. V. Prishchepov, "Effects of building density on land surface temperature in China: Spatial patterns and determinants," *Landscape Urban Plan.*, vol. 198, Jun. 2020, Art. no. 5003114, doi: 10.1016/j.landurbplan.2020.103794.

[13] B. H. Liu, Q. Zhan, S. Gao, R. Li, and Z. Fan, "The influence of urban form on surface urban heat island and its planning implications: Evidence from 1288 urban clusters in China," *Sustain. Cities Soc.*, vol. 71, Aug. 2021, Art. no. 102987, doi: 10.1016/j.scs.2021.102987.

[14] J. Chen, K. Yang, Y. Zhu, and F. Su, "Analysis of the relationship between land surface temperature and land cover types—A case study of Dianchi Basin," in *Proc. 23rd Int. Conf. Geoinform.*, 2015, pp. 1–6, doi: 10.1109/GEOINFORMATICS.2015.7378685.

[15] Z. L. Li et al., "Satellite remote sensing of global land surface temperature: Definition, methods, products, and applications," *Rev. Geophys.*, vol. 61, no. 1, 2023, Art. no. e2022RG000777, doi: 10.1029/2022RG000777.

[16] W. R. Johnson, S. J. Hook, W. P. Schmitigal, R. Gullioud, T. L. Logan, and K. T.Lum, "ECOSTRESS end-to-end radiometric validation," in *Proc. IEEE Aerosp. Conf.*, 2019, pp. 1–8, doi: 10.1109/AERO.2019.8741652.

[17] J. Zhu and H. Ren, "Feasibility of retrieving land surface temperature from ECOSTRESS data using split-window algorithms," *IEEE Geosci. Remote Sens. Lett.*, vol. 20, 2023, Art. no. 7001505, doi: 10.1109/LGRS.2023.3328664.

[18] S. J. Hook et al., "In-flight validation of the ECOSTRESS, Landsats 7 and 8 thermal infrared spectral channels using the lake Tahoe CA/NV and Salton Sea CA automated validation sites," *IEEE Trans. Geosci. Remote Sens.*, vol. 58, no. 2, pp. 1294–1302, Feb. 2020, doi: 10.1109/TGRS.2019.2945701.

[19] C. Guo, "Multi-scale analysis of diurnal changes in urban thermal environment," M.S. thesis, Dept. Sch. Geographical Sci. Remote Sens., Guangzhou Univ., Guangzhou, China, 2024, doi: 10.27040/d.cnki.ggzdu.2023.002145.

[20] Z. Lin, H. Xu, L. Han, H. Zhang, J. Peng, and X. Yao, "Day and night: Impact of 2D/3D urban features on land surface temperature and their spatiotemporal non-stationary relationships in urban building spaces," *Sustain. Cities Soc.*, vol. 108, Aug. 2024, Art. no. 105507, doi: 10.1016/j.scs.2024.105507.

[21] W. Shi, J. Hou, X. Shen, and R. Xiang, "Exploring the spatio-temporal characteristics of urban thermal environment during hot summer days: A case study of Wuhan, China," *Remote Sens.*, vol. 14, no. 23, Jan. 2022, Art. no. 6084, doi: 10.3390/rs14236084.

[22] A. Lin, H. Wu, W. Luo, K. Fan, and H. Liu, "How does urban heat island differ across urban functional zones? Insights from 2D/3D urban morphology using geospatial big data," *Urban Climate*, vol. 53, Jan. 2024, Art. no. 101787, doi: 10.1016/j.uclim.2023.101787.

[23] J. Yang et al., "Local climate zone ventilation and urban land surface temperatures: Towards a performance-based and wind-sensitive planning proposal in megacities," *Sustain. Cities Soc.*, vol. 47, May 2019, Art. no. 101487, doi: 10.1016/j.scs.2019.101487.

[24] B. Yuan, L. Zhou, X. Dang, D. Sun, F. Hu, and H. Mu, "Separate and combined effects of 3D building features and urban green space on land surface temperature," *J. Environ. Manage.*, vol. 295, Oct. 2021, Art. no. 113116, doi: 10.1016/j.jenvman.2021.113116.

[25] Z. Ding, J. Gu, D. Zeng, and X. Wang, "Effects of 'Inhaling' and 'Exhaling' of buildings in three-dimensional built environment on land surface temperature," *Building Environ.*, vol. 246, Dec. 2023, Art. no. 110930, doi: 10.1016/j.buildenv.2023.110930.

[26] S. Han et al., "Seasonal effects of urban morphology on land surface temperature in a three-dimensional perspective: A case study in Hangzhou, China," *Building Environ.*, vol. 228, Jan. 2023, Art. no. 109913, doi: 10.1016/j.buildenv.2022.109913.

[27] R. Fan, R. Feng, W. Han, and L. Wang, "Urban functional zone mapping with a bibranch neural network via fusing remote sensing and social sensing data," *IEEE J. Sel. Top. Appl. Earth Observ. Remote Sens.*, vol. 14, pp. 11737–11749, 2021, doi: 10.1109/JSTARS.2021.3127246.

[28] X. Huang, J. Yang, J. Li, and D. Wen, "Urban functional zone mapping by integrating high spatial resolution nighttime light and daytime multi-view imagery," *ISPRS J. Photogrammetry Remote Sens.*, vol. 175, pp. 403–415, May 2021, doi: 10.1016/j.isprsjprs.2021.03.019.

[29] J. Guo, G. Han, Y. Xie, Z. Cai, and Y. Zhao, "Exploring the relationships between urban spatial form factors and land surface temperature in mountainous area: A case study in Chongqing city, China," *Sustain. Cities Soc.*, vol. 61, Oct. 2020, Art. no. 102286, doi: 10.1016/j.scs.2020.102286.

[30] X. Qiao, Y. Li, Y. Wang, L. Liu, and S. Zhao, "The influence of climate and human factors on a regional heat island in the Zhengzhou metropolitan area, China," *Environ Res.*, vol. 249, May 2024, Art. no. 118331, doi: 10.1016/j.envres.2024.118331.

[31] X. Yao, Z. Zhu, X. Zhou, Y. Shen, X. Shen, and Z. Xu, "Investigating the effects of urban morphological factors on seasonal land surface temperature in a 'Furnace city' from a block perspective," *Sustain. Cities Soc.*, vol. 86, Nov. 2022, Art. no. 104165, doi: 10.1016/j.scs.2022.104165.

[32] M. Cai, C. Ren, and Y. Xu, "Investigating the relationship between local climate zone and land surface temperature," in *Proc. Joint Urban Remote Sens. Event*, 2017, pp. 1–4, doi: 10.1109/JURSE.2017.7924622.

[33] X. Ma et al., "XGBoost-based analysis of the relationship between urban 2-D/3-D morphology and seasonal gradient land surface temperature," *IEEE J. Sel. Top. Appl. Earth Observ. Remote Sens.*, vol. 17, pp. 4109–4124, 2024, doi: 10.1109/JSTARS.2023.3348476.

[34] H. An, H. Cai, X. Xu, Z. Qiao, and D. Han, "Impacts of urban green space on land surface temperature from urban block perspectives," *Remote Sens.*, vol. 14, no. 18, 2022, Art. no. 4580.

[35] H. Yang, W. Xu, E. Shao, Y. Liao, and X. Lin, "Research on spatial differentiation of urban functional zone effects based on warming index," *Trop. Geographer*, vol. 44, no. 3, pp. 557–568, 2024.

[36] L. Yao, Y. Xu, and B. Zhang, "Effect of urban function and landscape structure on the urban heat island phenomenon in Beijing, China," *Landscape Ecol. Eng.*, vol. 15, no. 4, pp. 379–390, Oct. 2019, doi: 10.1007/s11355-019-00388-5.

[37] S. Chen, D. Haase, S. Qureshi, and M. K. Firozjaei, "Integrated land use and urban function impacts on land surface temperature: Implications on urban heat mitigation in Berlin with eight-type spaces," *Sustain. Cities Soc.*, vol. 83, Aug. 2022, Art. no. 103944, doi: 10.1016/j.scs.2022.103944.

[38] J. Qiu, X. Li, and W. Qian, "Optimizing the spatial pattern of the cold island to mitigate the urban heat island effect," *Ecol. Indicators*, vol. 154, Oct. 2023, Art. no. 110550, doi: 10.1016/j.ecolind.2023.110550.

[39] D. Han et al., "Understanding seasonal contributions of urban morphology to thermal environment based on boosted regression tree approach," *Building Environ.*, vol. 226, Dec. 2022, Art. no. 109770, doi: 10.1016/j.buildenv.2022.109770.

[40] L. J. Hamberg, J. B. Fisher, J. L. W. Ruppert, J. Tureček, D. H. Rosen, and P. M. A. James, "Assessing and modeling diurnal temperature buffering and evapotranspiration dynamics in forest restoration using ECOSTRESS thermal imaging," *Remote Sens. Environ.*, vol. 280, Oct. 2022, Art. no. 113178, doi: 10.1016/j.rse.2022.113178.

[41] A. Lin et al., "Identifying urban building function by integrating remote sensing imagery and POI data," *IEEE J. Sel. Top. Appl. Earth Observ. Remote Sens.*, vol. 14, pp. 8864–8875, 2021, doi: 10.1109/JSTARS.2021.3107543.

[42] H. Bao, D. Ming, Y. Guo, K. Zhang, K. Zhou, and S. Du, "DFCNN-based semantic recognition of urban functional zones by integrating remote sensing data and POI data," *Remote Sens.*, vol. 12, no. 7, Jan. 2020, Art. no. 1088, doi: 10.3390/rs12071088.

[43] C. Wang, Y. Li, and X. Shi, "Information mining for urban building energy models (UBEMs) from two data sources: OpenStreetMap and Baidu Map," *Building Simul.*, vol. 16, pp. 3369–3376, 2019, doi: 10.26868/25222708.2019.210545.

[44] J. Yang and X. Huang, "The 30 m annual land cover dataset and its dynamics in China from 1990 to 2019," *Earth Syst. Sci. Data*, vol. 13, no. 8, pp. 3907–3925, Aug. 2021, doi: 10.5194/essd-13-3907-2021.

[45] W. J. Tu, X. Zeng, and Q. Liu, "Aging tsunami coming: The main finding from China's seventh national population census," *Aging Clin. Exp. Res.*, vol. 34, no. 5, pp. 1159–1163, May 2022, doi: 10.1007/s40520-021-02017-4.

[46] J. Gu and W. Dong, "Identification and interaction analysis of urban functional areas based on multi-source data," *Geomatics Inf. Sci. Wuhan Univ.*, vol. 43, no. 7, pp. 1113–1121, Jul. 2018, doi: 10.13203/j.whugis20160192.

[47] Y. Cai, H. Zhang, P. Zheng, and W. Pan, "Quantifying the impact of land use/land cover changes on the urban heat island: A case study of the natural wetlands distribution area of Fuzhou City, China," *Wetlands*, vol. 36, no. 2, pp. 285–298, Apr. 2016, doi: 10.1007/s13157-016-0738-7.

[48] H. Liu et al., "Recognizing urban functional zones by a hierarchical fusion method considering landscape features and human activities," *Trans. GIS*, vol. 24, no. 5, pp. 1359–1381, 2020, doi: 10.1111/tgis.12642.

[49] Y. Jing, R. Sun, and L. Chen, "A method for identifying urban functional zones based on landscape types and human activities," *Sustainability*, vol. 14, no. 7, Jan. 2022, Art. no. 4130, doi: 10.3390/su14074130.

[50] X. Yao et al., "Exploring the diurnal variations of the driving factors affecting block-based LST in a 'Furnace city' using ECOSTRESS thermal imaging," *Sustain. Cities Soc.*, vol. 98, 2023, Art. no. 104841.

[51] C. Huang, C. Xiao, and L. Rong, "Integrating point-of-interest density and spatial heterogeneity to identify urban functional areas," *Remote Sens.*, vol. 14, no. 17, Jan. 2022, Art. no. 4201, doi: 10.3390/rs14174201.

[52] Q. Qin, S. Xu, M. Du, and S. Li, "Urban functional zone identification by considering the heterogeneous distribution of points of interests," *ISPRS Ann. Photogrammetry, Remote Sens. Spatial Inf. Sci.*, vol. 4, pp. 83–90, May 2022, doi: 10.5194/isprs-annals-V-4-2022-83-2022.

[53] R. Wu, "Spatial differentiation of influencing factors on heat islands in the Beijing-Tianjin-Hebei urban agglomeration from the perspective of functional blocks," M.S. thesis, Dept. Sch. Public Admin., China Univ. Geosci., Beijing, China, 2022, doi: 10.27493/d.cnki.gzdzy.2021.000312.

[54] E. Zhu, J. Yao, X. Zhang, and L. Chen, "Explore the spatial pattern of carbon emissions in urban functional zones: A case study of Pudong, Shanghai, China," *Environ. Sci. Pollut. Res.*, vol. 31, no. 2, pp. 2117–2128, Dec. 2023, doi: 10.1007/s11356-023-31149-5.

[55] K. Cawse-Nicholson et al., "Sensitivity and uncertainty quantification for the ECOSTRESS evapotranspiration algorithm—DisALEXI," *Int. J. Appl. Earth Observ. Geoinf.*, vol. 89, Jul. 2020, Art. no. 102088, doi: 10.1016/j.jag.2020.102088.

[56] G. C. Hulley et al., "Validation and quality assessment of the ECOSTRESS level-2 land surface temperature and emissivity product," *IEEE Trans. Geosci. Remote Sens.*, vol. 60, 2022, Art. no. 5000523, doi: 10.1109/TGRS.2021.3079879.

[57] H. Jaafar, R. Mourad, and M. Schull, "A global 30-m ET model (HSEB) using harmonized Landsat and Sentinel-2, MODIS and VIIRS: Comparison to ECOSTRESS ET and LST," *Remote Sens. Environ.*, vol. 274, Jun. 2022, Art. no. 112995, doi: 10.1016/j.rse.2022.112995.

[58] J. Yang, Y. Yang, D. Sun, C. Jin, and X. Xiao, "Influence of urban morphological characteristics on thermal environment," *Sustain. Cities Soc.*, vol. 72, Sep. 2021, Art. no. 103045, doi: 10.1016/j.scs.2021.103045.

[59] D. Han et al., "How do 2D/3D urban landscapes impact diurnal land surface temperature: Insights from block scale and machine learning algorithms," *Sustain. Cities Soc.*, vol. 99, Dec. 2023, Art. no. 104933, doi: 10.1016/j.scs.2023.104933.

[60] L. Shao, W. Liao, P. Li, M. Luo, X. Xiong, and X. Liu, "Drivers of global surface urban heat islands: Surface property, climate background, and 2D/3D urban morphologies," *Building Environ.*, vol. 242, Aug. 2023, Art. no. 110581, doi: 10.1016/j.buildenv.2023.110581.

[61] K. McGarigal, "Landscape pattern metrics," in *Encyclopedia of Environmetrics*. Hoboken, NJ, USA: Wiley, 2013.

[62] X. Wang, F. G. Blanchet, and N. Koper, "Measuring habitat fragmentation: An evaluation of landscape pattern metrics," *Methods Ecol. Evol.*, vol. 5, no. 7, pp. 634–646, Jul. 2014, doi: 10.1111/2041-210X.12198.

[63] S. T. Mansouri and E. Zarghami, "Investigating the effect of the physical layout of the architecture of high-rise buildings, residential complexes, and urban heat islands," *Energy Built Environ.*, vol. 6, no. 1, pp. 1–17, Feb. 2025, doi: 10.1016/j.enbenv.2023.07.004.

[64] J. Wang, M. Fei, H. Lu, Y. Lv, and T. Jing, "Individual and combined effects of 3D buildings and green spaces on the urban thermal environment: A case study in Jinan, China," *Atmosphere*, vol. 14, May 2023, Art. no. 908, doi: 10.3390/atmos14060908.

[65] G. Kim, D.-H. Cha, C.-K. Song, and H. Kim, "Impacts of anthropogenic heat and building height on urban precipitation over the Seoul metropolitan area in regional climate modeling," *J. Geophys. Res.: Atmos.*, vol. 126, no. 23, 2021, Art. no. e2021JD035348, doi: 10.1029/2021JD035348.

[66] K. Do, "Computational and geo-spatial approaches to investigate multi-scale air quality trends in Southern California," Univ. California, Riverside, CA, USA, 2023. Accessed: Aug. 8, 2024. [Online]. Available: https://escholarship.org/uc/item/57f7q6hv

[67] J. Elith, J. R. Leathwick, and T. Hastie, "A working guide to boosted regression trees," *J. Animal Ecol.*, vol. 77, no. 4, pp. 802–813, 2008, doi: 10.1111/j.1365-2656.2008.01390.x.

[68] H. Ebrahimy, B. Feizizadeh, S. Salmani, and H. Azadi, "A comparative study of land subsidence susceptibility mapping of Tasuj plane, Iran, using boosted regression tree, random forest and classification and regression tree methods," *Environ. Earth Sci.*, vol. 79, no. 10, May 2020, Art. no. 223, doi: 10.1007/s12665-020-08953-0.

[69] T. A. Hallman and W. D. Robinson, "Comparing multi- and single-scale species distribution and abundance models built with the boosted regression tree algorithm," *Landscape Ecol.*, vol. 35, no. 5, pp. 1161–1174, May 2020, doi: 10.1007/s10980-020-01007-7.

[70] Y. Hu, Z. Dai, and J.-M. Guldmann, "Modeling the impact of 2D/3D urban indicators on the urban heat island over different seasons: A boosted regression tree approach," *J. Environ. Manage.*, vol. 266, Jul. 2020, Art. no. 110424, doi: 10.1016/j.jenvman.2020.110424.

[71] F. Sun, A. Mejia, and Y. Che, "Disentangling the contributions of climate and basin characteristics to water yield across spatial and temporal scales in the Yangtze river basin: A combined hydrological model and boosted regression approach," *Water Resour. Manage.*, vol. 33, no. 10, pp. 3449–3468, Aug. 2019, doi: 10.1007/s11269-019-02310-y.

[72] P. C. Ibsen, G. D. Jenerette, T. Dell, K. J. Bagstad, and J. E. Diffendorfer, "Urban landcover differentially drives day and nighttime air temperature across a semi-arid city," *Sci. Total Environ.*, vol. 829, Jul. 2022, Art. no. 154589, doi: 10.1016/j.scitotenv.2022.154589.

[73] A. Mathew, S. Khandelwal, and N. Kaul, "Analysis of diurnal surface temperature variations for the assessment of surface urban heat island effect over Indian cities," *Energy Buildings*, vol. 159, pp. 271–295, Jan. 2018, doi: 10.1016/j.enbuild.2017.10.062.

[74] J. Quan, "Diurnal land surface temperature characteristics of local climate zones: A case study in Beijing, China," in *Proc. IEEE Int. Geosci. Remote Sens. Symp.*, 2019, pp. 7443–7446, doi: 10.1109/IGARSS.2019.8898456.

[75] A. Mathew, S. Khandelwal, N. Kaul, and S. Chauhan, "Analyzing the diurnal variations of land surface temperatures for surface urban heat island studies: Is time of observation of remote sensing data important?," *Sustain. Cities Soc.*, vol. 40, pp. 194–213, Jul. 2018, doi: 0.1016/j.scs.2018.03.032.

[76] Z. Cai, G. Han, and M. Chen, "Do water bodies play an important role in the relationship between urban form and land surface temperature?," *Sustain. Cities Soc.*, vol. 39, pp. 487–498, May 2018, doi: 10.1016/j.scs.2018.02.033.

[77] Y.-C. Chen, H.-W. Chiu, Y.-F. Su, Y.-C. Wu, and K.-S. Cheng, "Does urbanization increase diurnal land surface temperature variation? Evidence and implications," *Landscape Urban Plan.*, vol. 157, pp. 247–258, Jan. 2017, doi: 10.1016/j.landurbplan.2016.06.014.

[78] Y. Bai, L. Liu, J. Yang, J. Wang, and Q. Zou, "Drivers of land surface temperatures from the perspective of urban functional zones," *IEEE J. Sel. Top. Appl. Earth Observ. Remote Sens.*, vol. 17, pp. 12274–12285, 2024, doi: 10.1109/JSTARS.2024.3416184.

[79] Z. Yu, Y. Jing, G. Yang, and R. Sun, "A new urban functional zone-based climate zoning system for urban temperature study," *Remote Sens.*, vol. 13, no. 2, Jan. 2021, Art. no. 251, doi: 10.3390/rs13020251.

[80] Y. Chen, J. Yang, R. Yang, X. Xiao, and J. C. Xia, "Contribution of urban functional zones to the spatial distribution of urban thermal environment," *Building Environ.*, vol. 216, 2022, Art. no. 109000.

[81] Z. Lin, H. Xu, X. Yao, C. Yang, and D. Ye, "How does urban thermal environmental factors impact diurnal cycle of land surface temperature? A multi-dimensional and multi-granularity perspective," *Sustain. Cities Soc.*, vol. 101, Feb. 2024, Art. no. 105190, doi: 10.1016/j.scs.2024.105190.

[82] Y. Lu, W. Yue, Y. Liu, and Y. Huang, "Investigating the spatiotemporal non-stationary relationships between urban spatial form and land surface temperature: A case study of Wuhan, China," *Sustain. Cities Soc.*, vol. 72, Sep. 2021, Art. no. 103070, doi: 10.1016/j.scs.2021.103070.

[83] Z. Li and D. Hu, "Exploring the relationship between the 2D/3D architectural morphology and urban land surface temperature based on a boosted regression tree: A case study of Beijing, China," *Sustain. Cities Soc.*, vol. 78, Mar. 2022, Art. no. 103392, doi: 10.1016/j.scs.2021.103392.

[84] Y. Chang et al., "Exploring diurnal thermal variations in urban local climate zones with ECOSTRESS land surface temperature data," *Remote Sens. Environ.*, vol. 263, 2021, Art. no. 112544.
[85] Y. Liu et al., "Exploring the seasonal effects of urban morphology on land surface temperature in urban functional zones," *Sustain. Cities Soc.*, vol. 103, Apr. 2024, Art. no. 105268, doi: 10.1016/j.scs.2024.105268.
[86] Y. Chen, J. Yang, W. Yu, J. Ren, X. Xiao, and J. C. Xia, "Relationship between urban spatial form and seasonal land surface temperature under different grid scales," *Sustain. Cities Soc.*, vol. 89, Feb. 2023, Art. no. 104374, doi: 10.1016/j.scs.2022.104374.
[87] G. Suthar, S. Singh, N. Kaul, and S. Khandelwal, "Prediction of land surface temperature using spectral indices, air pollutants, and urbanization parameters for Hyderabad city of India using six machine learning approaches," *Remote Sens. Appl.: Soc. Environ.*, vol. 35, Aug. 2024, Art. no. 101265, doi: 10.1016/j.rsase.2024.101265.
[88] Y. Chen, B. Shan, and X. Yu, "Study on the spatial heterogeneity of urban heat islands and influencing factors," *Building Environ.*, vol. 208, Jan. 2022, Art. no. 108604, doi: 10.1016/j.buildenv.2021.108604.
[89] A. Guo, W. Yue, J. Yang, and T. He, "Divergent impact of urban 2D/3D morphology on thermal environment along urban gradients," *Urban Climate*, vol. 45, Sep. 2022, Art. no. 101278, doi: 10.1016/j.uclim.2022.101278.
[90] D. Danniswari, T. Honjo, A. Kato, and K. Furuya, "Utilizing open-source satellite data for the relationship between building height and land surface temperature," *J. Environ. Inf. Sci.*, vol. 2021, no. 2, pp. 1–10, 2022, doi: 10.11492/ceispapersen.2021.2_1.
[91] W. Liao, T. Hong, and Y. Heo, "The effect of spatial heterogeneity in urban morphology on surface urban heat islands," *Energy Buildings*, vol. 244, Aug. 2021, Art. no. 111027, doi: 10.1016/j.enbuild.2021.111027.
[92] Y. Mo, Y. Bao, Z. Wang, W. Wei, and X. Chen, "Spatial coupling relationship between architectural landscape characteristics and urban heat island in different urban functional zones," *Building Environ.*, vol. 257, Jun. 2024, Art. no. 111545, doi: 10.1016/j.buildenv.2024.111545.

Qianmin Zhang received the bachelor's degree in urban planning in 2023 from Jangho Architecture College, Northeastern University, Shenyang, China, where she is currently working toward the master's degree in urban and rural planning.

Her research interests include urban planning, urban thermal environment, and urban function zone.

Jun Yang received the Ph.D. degree in urban human settlements from Liaoning Normal University, Dalian, China, in 2009.

He is currently a Professor in the effect of human settlement and GIS with Liaoning Normal University and a Professor with Jiangho Architecture, Northeastern University, Shenyang, China. His research interests include urban space growth, urban thermal environmental, cellular automata land use change, urban human settlements, as well as other aspects of research.

Xinyue Ma received the bachelor's degree in urban and rural planning from Jangho Architecture, Northeastern University, Shenyang, China, in 2021, where she is currently working toward the master's degree.

Her research interests include urban planning, urban climate, and carbon emissions.

Jiaxing Xin is working toward the Ph.D. degree in land resources management with Northeastern University, Shenyang, China.

Her research interests include urban thermal environment, land use policy, and local climate zone.

Jiayi Ren is working toward the Ph.D. degree in land resources management with Northeastern University, Shenyang, China.

Her research interests include assessment of urban thermal environment and land use policy.

Wenbo Yu is working toward the Ph.D. degree in land resources management with Northeastern University, Shenyang, China.

His current research interests include space-time evolution of human settlements, urban thermal environment, and urban landscape analysis.

Xiangming Xiao received the Ph.D. degree in ecology from Colorado State University, Fort Collins, CO, USA, in 1994.

He is currently a Professor with the School of Biological Sciences, University of Oklahoma, Norman, OK, USA, and the Director of the Earth Observation and Modeling Office. His research interests include land use and land cover change, the carbon cycle, and ecological environment analysis of infectious diseases.

Jianhong Xia received the Ph.D. degree in geographic information science from Liaoning Normal University, Dalian, China, in 1996.

She is currently a Professor with the School of Earth and Planetary Sciences, Curtin University, Perth, WA, Australia. She has worked as a Transport Geographer and Transit Planner with a range of research experience in relation to tourism, public transport development, driving, spatial navigation and way finding, and human mobility.